

**Development of a series of quinazoline-2,5-diamine derivatives
as potent hematopoietic progenitor kinase 1 (HPK1) inhibitors**

Huanyu Shi^{a,c,#}, Haotian Tang^{b,c,#}, Yan Li^{b,c,#}, Danqi Chen^a, Tongchao Liu^a, Yuting Chen^{a,c}, Xin Wang^a, Lin Chen^a, Ying Wang^a, Hua Xie^{b,c,d,*}, Bing Xiong^{a,c,*}

^a *Department of Medicinal Chemistry, Shanghai Institute of Materia Medica, Chinese Academy of Sciences, Shanghai 201203, China*

^b *Division of Antitumor Pharmacology, State Key Laboratory of Drug Research, Shanghai Institute of Materia Medica, Chinese Academy of Sciences, China*

^c *University of Chinese Academy of Sciences, Beijing 100049, P. R. China*

^d *Zhongshan Institute for Drug Discovery, Shanghai Institute of Materia Medica, Chinese Academy of Sciences, Zhongshan 528400, China*

[#]These authors contributed equally.

^{*}Corresponding authors.

Email address: bxiong@simm.ac.cn (B. Xiong), hxie@simm.ac.cn (H. Xie).

Abstract

Hematopoietic progenitor kinase 1 (HPK1) is a serine/threonine kinase that serves as the negative regulator of multiple immune signaling pathways. Genetic studies using HPK1 knockout and kinase-dead mice suggested that inhibiting HPK1 either alone or in combination with immune checkpoint blockade could be promising strategy in cancer immunotherapy. Herein, we report the design, synthesis and structure–activity relationship (SAR) study of a series of potent HPK1 inhibitors bearing quinazoline-2,5-diamine scaffold. Three rounds of SAR explorations led to the identification of **9h**, the most potent compound in this series which harbors a 2-methyl-1,2,3,4-tetrahydroisoquinolin-7-yl substituent. Further biological studies using human immune cells demonstrated that **9h** could strongly inhibit the downstream phosphorylation, augment the IL-2 secretion and reverse the PGE2-induced immune suppression. Overall, **9h** can serve as a tool compound to help with demonstrating the pharmacological role of HPK1 kinase inhibition, and our investigation provided a reliable reference for the later development of HPK1 inhibitors.

Keywords: Cancer immunotherapy; SAR study; HPK1 inhibitors; Quinazoline-2,5-diamine; IL-2 secretion.

1. Introduction

In the last decade, immunotherapy has significantly changed the landscape of cancer treatment[1, 2]. As representatives, antibodies targeting immune checkpoints, such as programmed cell death-1 (PD-1) inhibitors and programmed cell death-ligand 1 (PD-L1) inhibitors, have won great clinical success in treating various cancer indications[3-7]. However, due to the complicated immune resistance mechanisms, these immune checkpoint inhibitors can only benefit a subset of patients[8-10]. Thus, there is an urgent need to search for other immune negative regulators that can serve as complementary or alternative drug targets[8, 11-13].

Hematopoietic progenitor kinase 1 (HPK1), also termed as mitogen-activated protein kinase kinase kinase kinase 1 (MAP4K1), is a serine/threonine kinase that mainly expressed in hematopoietic cells[14, 15]. As an immune negative regulator, HPK1 suppresses the transduction of multiple signaling pathways in immune cells, among which the regulatory role in T cell receptor (TCR) signaling pathway was mostly studied[16-21]. Upon TCR stimulation, successive phosphorylations on Tyr381, Ser171 and Thr165 lead to the full activation of HPK1. Fully activated HPK1 then phosphorylates Src homology 2 domain containing leukocyte protein of 76 kDa (SLP76), a component of TCR signalosome, at Ser376. This process further causes the destabilization of TCR signalosome, and as a consequence, the transduction of TCR signaling is attenuated[14, 15]. Early knockout studies demonstrated that HPK1-deficient mice showed enhanced T cell proliferation, increased T helper type 1 (Th1) cytokine (e.g., IL-2, IFN- γ) production, and improved dendritic cell-mediated antigen

presentation[16, 21]. Later studies using HPK1 kinase-dead mice emphasized the predominant role of HPK1 kinase activity in regulating T cell function, and co-blocking the kinase activity of HPK1 and PD-1/PD-L1 axis could bring a synergetic antitumor effect in murine colon adenocarcinoma model[18]. Furthermore, T cells from the genetic engineered mice were resistant to immune suppression mediated by PGE2 and adenosine[17, 19]. Given these compelling evidences, together with the numerous successful cases in kinase drug discovery, HPK1 has been proposed as a promising target in cancer immunotherapy.

Discovery efforts paid by the pharmaceutical industry and academia have translated into the emergence of clinic HPK1 inhibitors. So far, five small-molecule compounds have advanced into clinical trials, however, their structures are undisclosed[22-27]. Meanwhile, a few ATP-competitive HPK1 inhibitors have been reported in recent literatures (**Fig. 1**). Reverse indazole compound **1** from Merck was well balanced between potency and kinase selectivity, but its efficacy in immune cells was not mentioned in the article[28]. Spiro-azaindoline inhibitor **2** discovered by Genetech displayed high binding affinity HPK1, and it could dose- dependently increase the IL-2 secretion of human pan T cells[29]. Diaminopyrimidine carboxamide derivative **3** from Merck exhibited excellent IC₅₀ values in biochemical and cell-based assays, but unfortunately, the unsatisfying pharmacokinetic (PK) property might impede it from oral administration[30]. Aminopyridine compound ZYF0033 (**4**) presented good *in vitro* activities, and it was effective *in vivo* when dosed intraperitoneally as well[31]. Finally, isofuranone derivative **5**, a potent and orally

active HPK1 inhibitor developed by Bristol-Myers Squibb, could markedly enhance the efficacy of PD-1 antibody in murine tumor model[32].

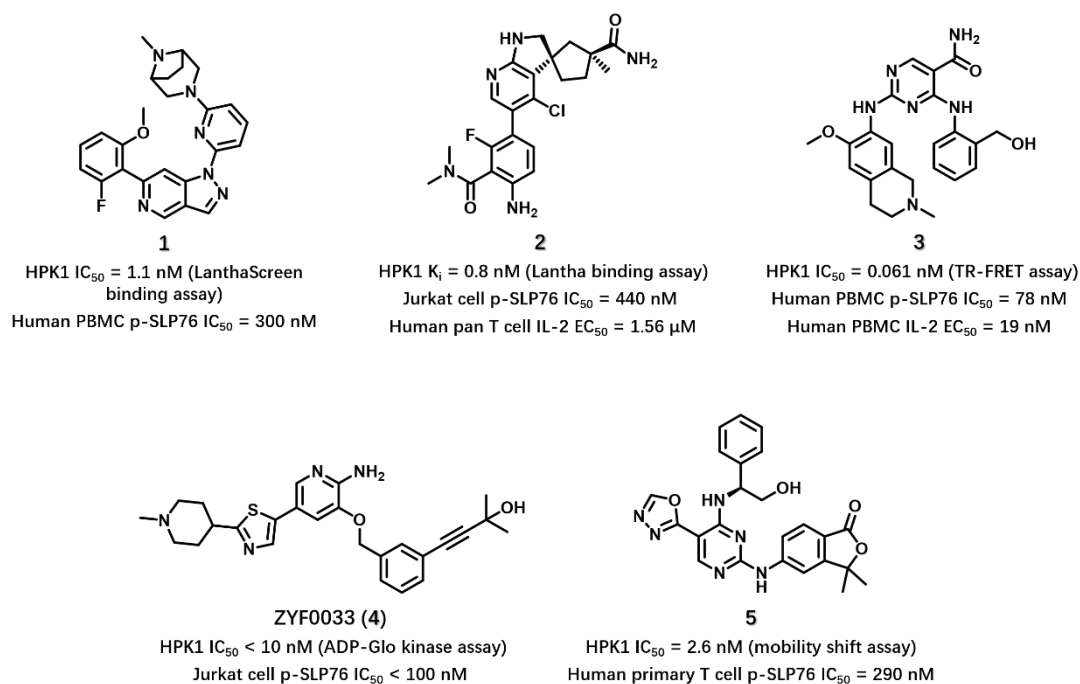


Fig. 1. Representative HPK1 inhibitors that reported in literatures.

Thus, for the development of HPK1 inhibitors, referable information is still limited, especially the detailed structure–activity relationship (SAR) explorations and biological evaluations of other chemotypes. Herein, we describe our efforts on the development of potent HPK1 inhibitors bearing quinazoline-2,5-diamine scaffold. We hope that our SAR explorations and the related biological evaluations will contribute to the drug discovery targeting HPK1.

2. Results and discussion

2.1. Rational design of quinazoline-2,5-diamine HPK1 inhibitors.

When investigating the literature-reported HPK1 inhibitors (**Fig. 1**), we found that there were usually large gaps between the enzymatic and cellular activities, which could

result from the low apparent ATP K_m of HPK1 (reported as 8.9 μM)[28, 33]. Thus, high potency might be of great importance for a HPK1 inhibitor to compete with high concentrations of cellular ATP so as to attain adequate target engagement. In light of this, we turned our attentions to a set of highly potent isoquinoline-3,8-diamine HPK1 inhibitors, which were previously disclosed in Genetech's patent and later reevaluated by Lacey *et al*[33, 34]. To better understand the binding mode of this chemotype, we selected compound **6** (**Fig. 2A**) as a representative and applied it to a molecular docking study. As **Fig. 2B** depicts, the docking model suggested a type I (DFG-in) binding mode, the isoquinoline-3,8-diamine hinge-binding motif could form classic donor-acceptor-donor hydrogen bonds with hinge residues Glu92 and Cys94, the nitrogen atom in 4-methylpyridine moiety could also interact with Lys46, and the cyclopropanecarbonyl group was positioned near the solvent-exposed region. Inspired by this amino-6,6-heterocyclic bicycle, we embedded a nitrogen atom in isoquinoline-3,8-diamine and generated the quinazoline-2,5-diamine skeleton (**Fig. 2C**). The subsequent SAR explorations would be performed at 2-amino group (substituent designated as R^1) and C7 position (substituent designated as R^2).

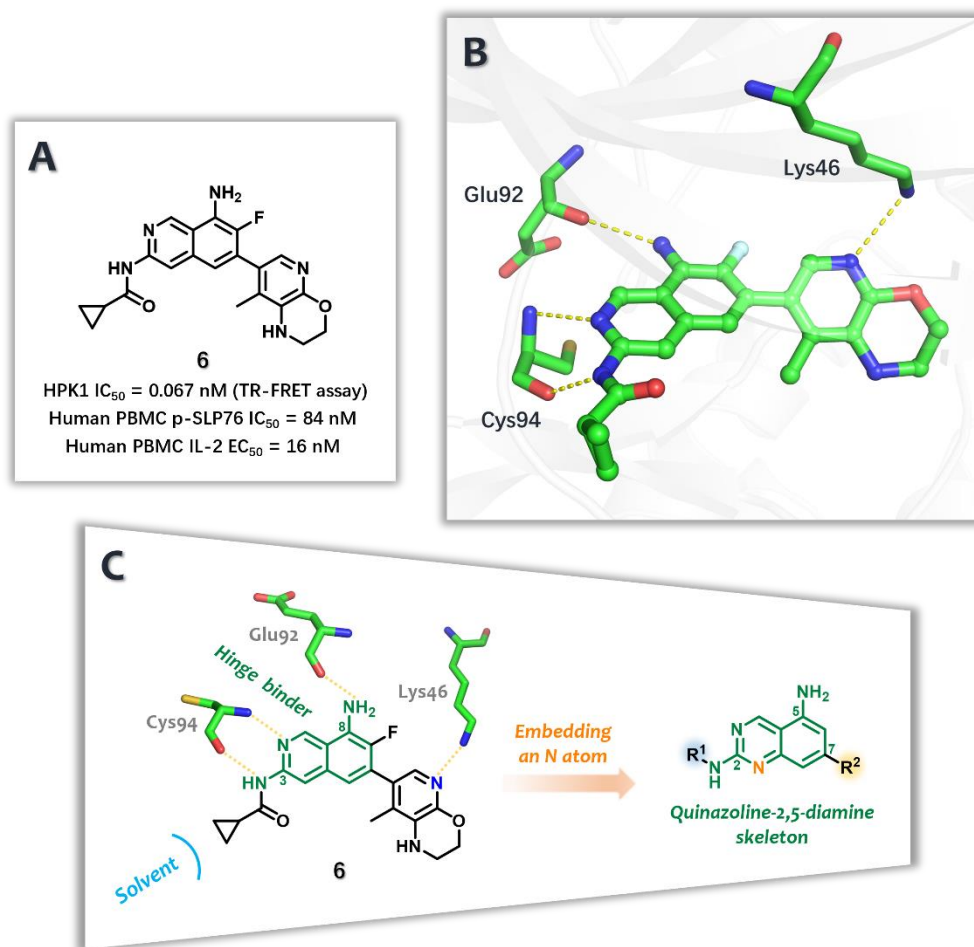


Fig. 2. (A) Chemical structure of compound **6**. (B) Predicted binding mode of **6** in the ATP-binding site of HPK1 (PDB code: 7L25). Hydrogen bonds are illustrated with yellow dash lines. (C) Design strategy for quinazoline-2,5-diamine HPK1 inhibitors.

Initially, to test the compatibility of carbonyl group with our quinazoline-2,5-diamine core, we synthesized **7a**—the quinazoline-2,5-diamine analogue of **6** (Table 1). Disappointingly, while the IC_{50} value of compound **6** was measured as 3.1 nM in our internal ADP-Glo kinase assay, **7a** exhibited an extremely low HPK1 inhibitory rate at 100 nM. To find out the intrinsic cause of such a great activity drop, we carried out a molecular modeling study using energy–dihedral angle scan, and the later result suggested a distinct conformational difference between **6** and **7a**. While the lowest

energy conformer of **6** harbored a *trans*-amide that identical to the predicted bioactive conformer (**Fig. 3A** and **Fig. 3B**), **7a** preferred to adopt a *cis*-conformation in its amide moiety (**Fig. 3C**). More importantly, conversion between the lowest energy conformation and bioactive conformation of **6** was free owing to the high similarity, however, the energy barrier was nearly 11.6 kcal/mol for **7a** to accomplish such a conformational change, which means the energy penalty for the binding of **7a** to HPK1 was much higher than that of **6** (when calculating, we assumed that the conformations of cyclopropanecarboxamide moiety in the bioactive conformer of **6** and **7a** were identical; see **Fig. S1** for the contour plot of potential energy of **6** and **7a**). We speculated that this conformational difference was attributed to repulsion of lone pair electrons between quinazoline N1 atom and amide O atom.

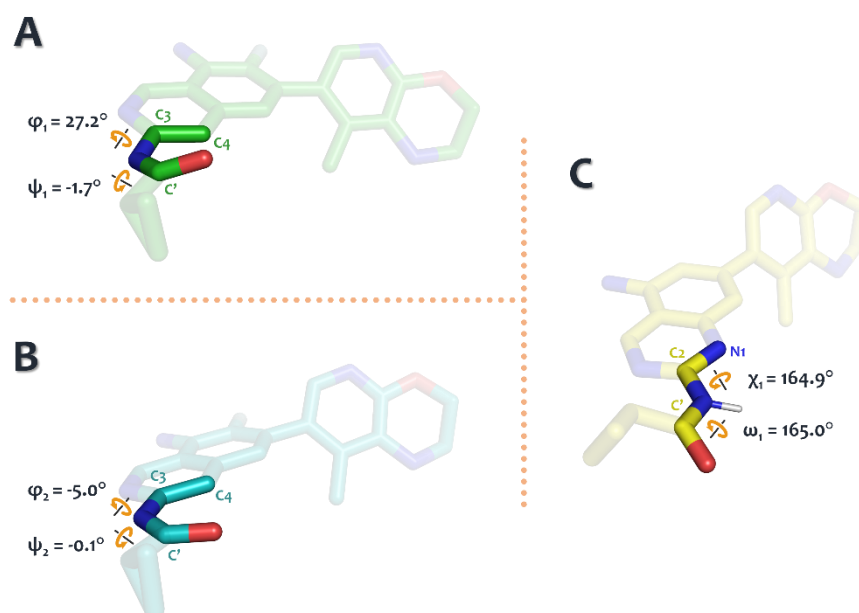


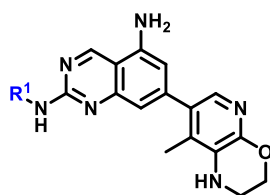
Fig. 3. (A) Bioactive conformation of **6** that predicted in the docking study, φ_1 and ψ_1 were measured as 27.2° and -1.7° respectively. (B) Lowest energy conformation of **6** that calculated in the energy–dihedral angle scan, φ_2 and ψ_2 were measured as -5.0° and -0.1° respectively. (C) Lowest energy conformation of **7a** that calculated in the energy–dihedral angle scan, χ_1 and ω_1 were measured as

164.9° and 165.0° respectively. Definitions of dihedral angles φ , ψ , χ and ω : φ : C4–C3–N–C', ψ : C3–N–C=O, χ : N1–C2–N–C', ω : C2–N–C'=O.

2.2. Preliminary exploration of R^1 .

In order to mitigate the lone pair repulsion and meanwhile maintain the carbonyl π bond property, we replaced the cyclopropanecarbonyl group with six- or five-membered heterocycles (**Table 1**). The activity of 2-pyridyl compound **7b** received a remarkable improvement since the probability of the repulsion was cut by half (the repulsion take place only when the pyridine N atom turn towards the quinazoline core). To thoroughly avoid the lone pair repulsion, we shifted this N atom to the *meta*- or *para*- position, and as expected, the resulting **7c** and **7d** displayed a single-digit nanomolar IC_{50} against HPK1. As representatives of five-membered rings, various pyrazolyl groups were also introduced. Among them, N-methylpyrazolyl were well tolerated (**7e** and **7f**), but prolonging the N-alkyl chains by one carbon unit could slightly erode the potencies (**7g** and **7h**). Furthermore, adding a methyl group to certain positions of the pyrazole ring could bring detrimental effects (**7j** vs **7e**, **7k** vs **7f**), and the activity was completely lost when the pyrazole ring was dimethylated (**7l**), which could be imputed to steric hindrances of the methyl groups that impeded the pyrazole ring from adopting the optimal conformation. Interestingly, during the subsequent examination on the more active 1*H*-pyrazol-4-yl group, we found that attaching bulkier alkyl groups to the pyrazole N atom could recover the strong inhibitory effects (**7m** and **7n**), especially the cyclopropyl group (**7m**, $IC_{50} = 5.7$ nM).

Table 1. *In vitro* HPK1 inhibitory activities of compounds **7a–7n**^a.



Cpds.	R ¹	HPK1 IC ₅₀ (nM)	Cpds.	R ¹	HPK1 IC ₅₀ (nM)
7a		4.7%@100 nM ^b	7i		7.9 ± 1.0
7b		95.7 ± 3.4	7j		53 ± 15.2
7c		5.5 ± 2.5	7k		35.7 ± 12.3
7d		5.7 ± 3.9	7l		7.5%@100 nM ^b
7e		12.7 ± 0.7	7m		5.7 ± 3.4
7f		7.8 ± 1.2	7n		6.4 ± 3.7
7g		15.5 ± 3.7	5 ^c	-	15.0 ± 6.3
7h		12.0 ± 8.6	6 ^c	-	3.1 ± 1.9

^aHPK1 inhibitory activities were determined using ADP-Glo kinase assay. The IC₅₀ values and inhibitory rates are mean values from at least two independent experiments. ^bHPK1 inhibitory rate at compound concentration of 100 nM. ^cPositive control.

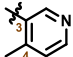
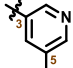
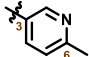
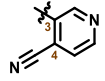
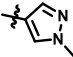
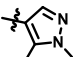
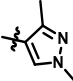
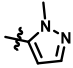
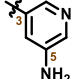
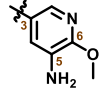
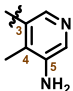
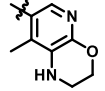
2.3. Exploration of R².

In consideration of the satisfying IC₅₀ of **7m**, along with the high synthetic accessibility for structural derivatization based on intermediate **28j** (see **Scheme 4** for detailed synthetic route), we tentatively kept R¹ as 1-cyclopropyl-1H-pyrazol-4-yl and explored the SAR at quinazoline C7 position (**Table 2**). When comparing the activities

of **8a–8d**, we noticed an apparent advantage for pyridin-3-yl compound **8c**, which supported the prediction of forming a hydrogen bond with Lys46. Incorporating a 4-methyl group to the pyridin-3-yl substituent could further boost the potency, yielding **8e** with an IC₅₀ value of 17.9 nM, and whether shifting or extending the length of this methyl group could result in nearly 10-fold decrease in potency (**8f–8h**). Thus, we considered that this methyl might force the pyridine ring to rotate by an angle from the quinazoline core, thereby assisting the hydrogen bond formation. As for N-methylpyrazole derivatives, **8i** and **8j** displayed moderate IC₅₀ values, but still about three-times weaker than the 4-methylpyridine counterpart **8e**. **8k** and **8l** were poor inhibitors in comparison with **8i** and **8j**, indicating that the methyl groups located between the activity-essential N atom and the attachment site were not tolerable.

Table 2. *In vitro* HPK1 inhibitory activities of compounds **8a–8o**^a.

Cpds.	R ²	HPK1 inhibitory rate (%)		HPK1 IC ₅₀ (nM)
		1 μM	100 nM	
8a		33.6	1.6	n.d. ^b
8b		30.3	-6.9	n.d.
8c		86.0	56.2	61.4 ± 22.8
8d		24.1	-3.3	n.d.

8e		98.1	87.2	17.9 ± 7.6
8f		87.6	42.7	n.d.
8g		85.9	36.2	n.d.
8h		85.5	36.3	n.d.
8i		95.8	68.6	50.5 ± 13.0
8j		90.9	53.6	61.1 ± 4.0
8k		25.8	-5.1	n.d.
8l		49.2	23.2	n.d.
8m		n.d.	80.0	33.2 ± 7.3
8n		60.6	0.1	n.d.
8o		n.d.	93.0	10.4 ± 5.1
7m		n.d.	96.3	5.7 ± 3.4
5^c	-	99.7	92.5	15.0 ± 6.3
6^c	-	n.d.	97.9	3.1 ± 1.9

^aHPK1 inhibitory activities were determined using ADP-Glo kinase assay. The IC₅₀ values and inhibitory rates are mean values from at least two independent experiments. ^bn.d. = not determined. ^cPositive control.

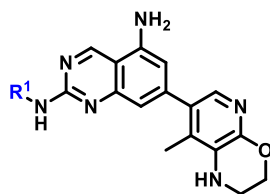
To investigate the role of the morpholine moiety in the original bicyclic substituent, we synthesized the 5-aminopyridin-3-yl compound **8m**, potency of which was doubled from **8e**. Unexpectedly, the activity dropped sharply when another 6-methoxy was introduced (**8n**), which reminded us that conformational restriction of this freely rotatable methoxy group was vital for the potency. The IC₅₀ value reached to 10.4 nM when both 4-methyl and 5-amino group were incorporated to the pyridine ring (**8o**), but despite such improvement, the original bicyclic substituent was still the optimal R² (**8o** vs **7m**).

2.4. Introducing aliphatic amines to R¹.

With the aim of further boosting the potency, we retained the optimal bicyclic R² substituent and turned our focus back to R¹, and this time, we would give priority to aryl substituents in view of their high feasibility for structural derivatization. As the starting point of derivatization, **9a** bearing a phenyl group as R¹ was synthesized (**Table 3**), and similar to its pyridyl counterpart **7c** and **7d**, **9a** presented a single-digit IC₅₀. In the subsequent docking study on **9a** (**Fig. 4A**), in addition to the anticipated identical binding pose to compound **6**, we also found that Asp101 near the phenyl ring might be utilized to produce an additional interaction, thereby contributing to the activity. To build polar contact with the acidic residue, we regarded aliphatic amine as an excellent choice because the its basic N atom could be easily protonated and interact with the carboxy anion *via* salt bridge interaction—a noncovalent interaction that stronger than

hydrogen bond[35].

Table 3. *In vitro* HPK1 inhibitory activities of compounds **9a–9l**^a.



Cpds.	R ¹	HPK1 IC ₅₀ (nM)	Cpds.	R ¹	HPK1 IC ₅₀ (nM)
9a		6.2 ± 5.0	9h		2.7 ± 2.2
9b		5.0 ± 1.5	9i		4.8 ± 0.8
9c		4.3 ± 0.9	9j		7.3 ± 5.4
9d		6.0 ± 1.9	9k		6.9 ± 4.3
9e		5.6 ± 2.6	9l		5.2 ± 0.9
9f		3.0 ± 1.3	5^b	-	15.0 ± 6.3
9g		4.3 ± 0.5	6^b	-	3.1 ± 1.9

^aHPK1 inhibitory activities were determined using ADP-Glo kinase assay. The IC₅₀ values and inhibitory rates are mean values from at least two independent experiments. ^bPositive control.

Based on this hypothesis, we designed and synthesized compounds **9b–9l** as can be seen in **Table 3**. According to the distances that measured in the docking model (**Fig. 4A**), we attached several aliphatic-amine-containing side chains to the 3- or 4- position of the phenyl ring, the resulting **9b–9e** were slightly more potent than phenyl compound

9a. To fix these N atoms to the optimal position, we locked them into six-membered rings and obtained tetrahydroisoquinoline compound **9f** and **9g**, among which **9f** showed furtherly enhanced potency that comparable to **6** and five-times more potent than **5**. Moreover, IC_{50} values were well maintained when these secondary amines were methylated (**9h** vs **9f**, **9i** vs **9g**), and **9h** which harbors a 2-methyl-1,2,3,4-tetrahydroisoquinolin-7-yl substituent exhibited an IC_{50} value of 2.7 nM. Further exploration based on **9h** was also conducted, but the activities of **9j–9l** revealed that bulkier N-alkyl groups or a 6-methoxy group in the tetrahydroisoquinoline moiety were not beneficial. Finally, to test our hypothesis of producing an additional interaction, we carried out a molecular docking study using the most potent **9h**. As Fig. 4B depicts, **9h** could maintain the key hydrogen bonds that predicted for **6** and **9a**, more importantly, this model suggested that the tetrahydroisoquinoline N atom could create salt bridge contact with Asp101, which provided a molecular explanation for the high potency of **9h**.

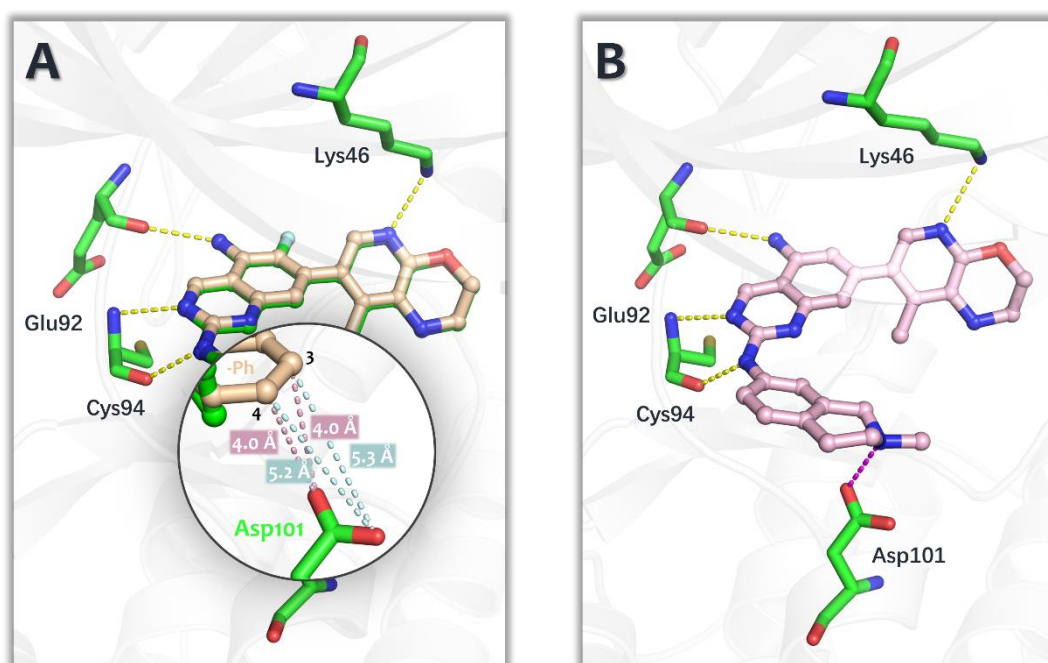


Fig. 4. (A) Predicted binding mode of **9a** (wheat) in the ATP-binding site of HPK1 and superimposition of **9a** with **6** (green). The distances between the phenyl C3 atom and two carboxy O atoms were measured as 4.0 Å and 5.3 Å respectively, and the distances between the phenyl C4 atom and two carboxy O atoms were measured as 4.0 Å and 5.2 Å respectively. (B) Predicted binding mode of **9h** in the ATP-binding site of HPK1. Hydrogen bonds are illustrated with yellow dash lines, measurements are illustrated with light-pink and pale-cyan dash lines, and salt bridge interaction is illustrated with magenta dash line.

2.5. Biological activity of **9h** targeting HPK1.

To further investigate the bioactivity of **9h**, we firstly performed target inhibitory test using human Jurkat cells coupled with **7m** developed in exploration of R¹ substituent. Jurkat cells are widely used in studies of TCR downstream signaling, and phosphorylation of SLP76 (pSLP76) at Ser376 is a reliable marker of HPK1 inhibition. We verified that Jurkat cell pSLP76 was activated by anti-CD3/28 sharply, and treated with a titration of doses of **7m** and **9h** both exhibited dose-dependent inhibition of pSLP76 in Jurkat cells (**Fig. 5**). It is worth noting that 33 nM of **7m** could significantly inhibit over 50% of pSLP76 relative to stimulation (**Fig. 5A**). Whereas **9h** boasted stronger inhibition of pSLP76 at only 3.7 nM than **7m**, and yielded an almost complete abolishment at 100 nM (**Fig. 5B**), defining **9h** as a high cellular activity HPK1 inhibitor.

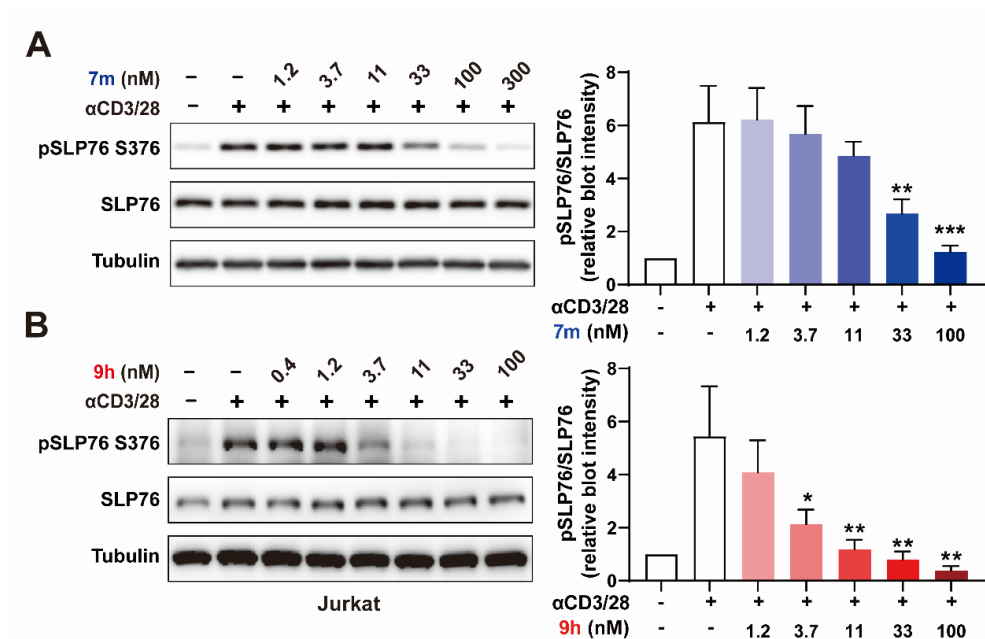


Fig.5 7m (A), and **9h** (B) inhibited pSLP76 S376 on anti-CD3/28 (α CD3/28) stimulated Jurkat cells. Representative Western Blots were shown and relative blot intensity of pSLP67/SLP76 from 4 independent replicates were analyzed and given in mean with SEM. Tubulin served as loading control. * $P < 0.05$, ** $P < 0.01$, *** $P < 0.001$.

As IL-2 production is a key marker indicating T cell activation, we next utilized human peripheral blood mononuclear cells (hPBMCs) to test the IL-2 production after administration of **7m**, **9h** and the positive control **6**. Under stimulation of anti-CD3/28, all 3 compounds elevated IL-2 production of hPBMCs at certain concentrations (**Fig. 6A**). Of which, **9h** exhibited the most potent activity in triggering IL-2 secretion of hPBMCs ranged from 0.03 to 0.3 μ M. Notably, a relative low dose of **9h** (0.03 μ M) was enough to boost the IL-2 production significantly ($P < 0.01$) and overwhelmed the promoting effects of **7m** and **6** under all doses. **9h** reached the peak of pro-IL-2 production effect at 0.3 μ M ($P < 0.001$) with a near 3-fold increase than the baseline stimulation, further proving its strong cellular activity.

Since hPBMCs derived from different donors usually exhibited discrepant

sensitivities, we paired the IL-2 production with or without compound treatment (0.3 μM) by each donor (**Fig. 6B**). Similarly, **7m** only slightly promoted IL-2 secretion ($P = 0.053$), while **9h** powerfully triggered IL-2 production ($P < 0.001$) and was more potent than **6**. These results indicated the promising activity of **9h** targeting HPK1 in hPBMCs.

Prostaglandin E2 (PGE2), a known immune-suppressive molecule, is able to restrain T cell activation and IL-2 production. We therefore tested whether **7m** and **9h** could overcome this repression. It was shown that 5 nM of PGE2 was able to abolish the IL-2 secretion of hPBMCs (**Fig. 6C**). Targeting HPK1 by 0.3 μM of **7m**, **9h** and **6** successfully released the abolished IL-2 production caused by PGE2, and reversed the IL-2 level back to that of no-PGE2 control, while **9h** exhibited a relatively highest effect (**Fig. 6C**).

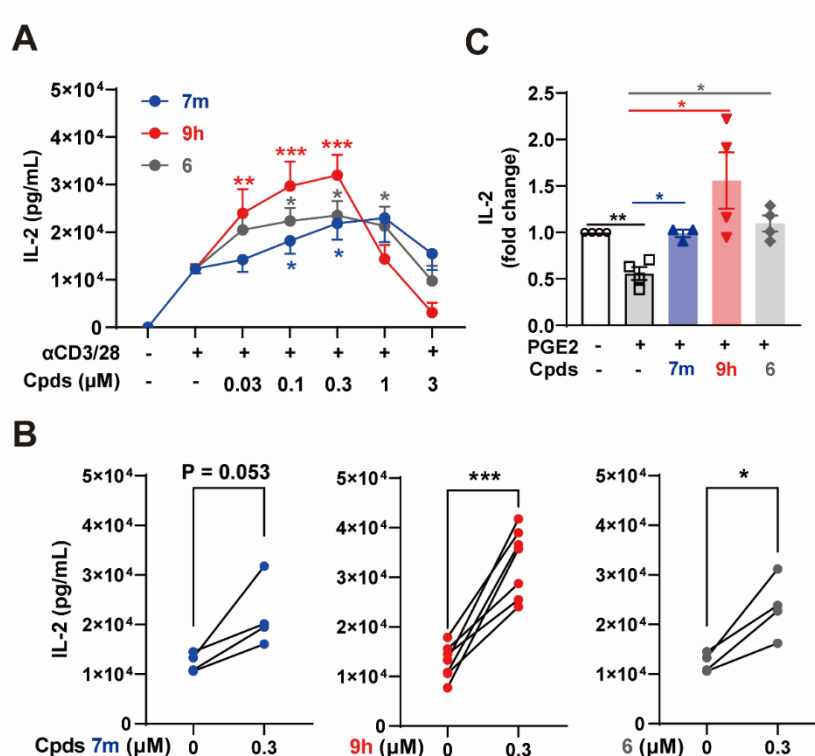


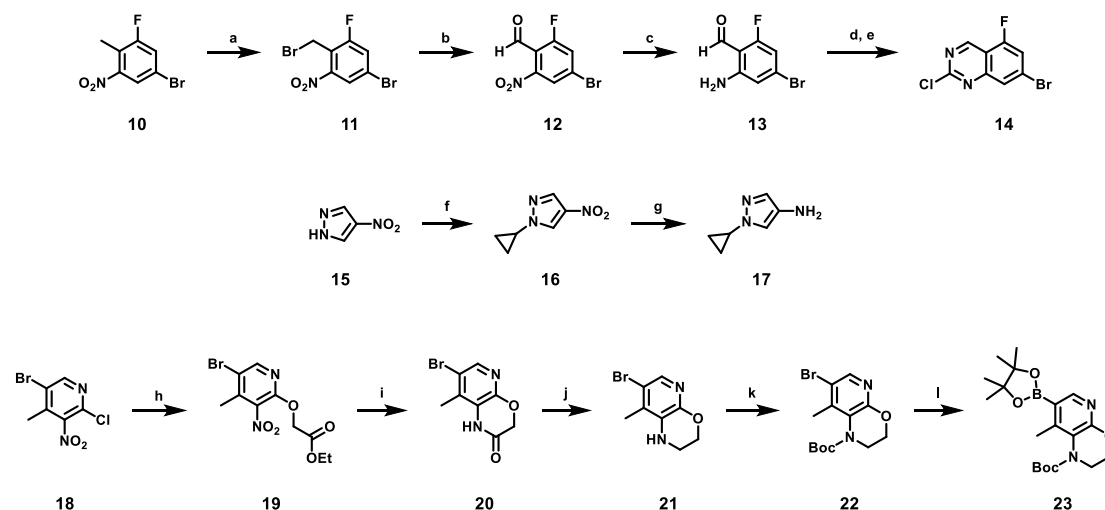
Fig. 6 IL-2 production in hPBMCs under treatments of **7m**, **9h** and **6** at indicated concentrations (A), and in paired hPBMCs donors (B). Fold change of IL-2 production (relative to no-PGE2 nor

compound control) in PGE2 pre-treated hPBMCs under 0.3 μ M of **7m**, **9h** and **6** (C). Data of **9h** paired effect were from seven independent tests, and the rest results were from four independent tests. Data in (A) and (B) were presented in mean with SEM. * P < 0.05, ** P < 0.01, *** P < 0.001.

Taken together, we verified that **9h** is a potent HPK1 inhibitor with high molecular activity, which shows promising cellular effects in both target inhibition of Jurkat cells and augment of IL-2 production of hPBMCs.

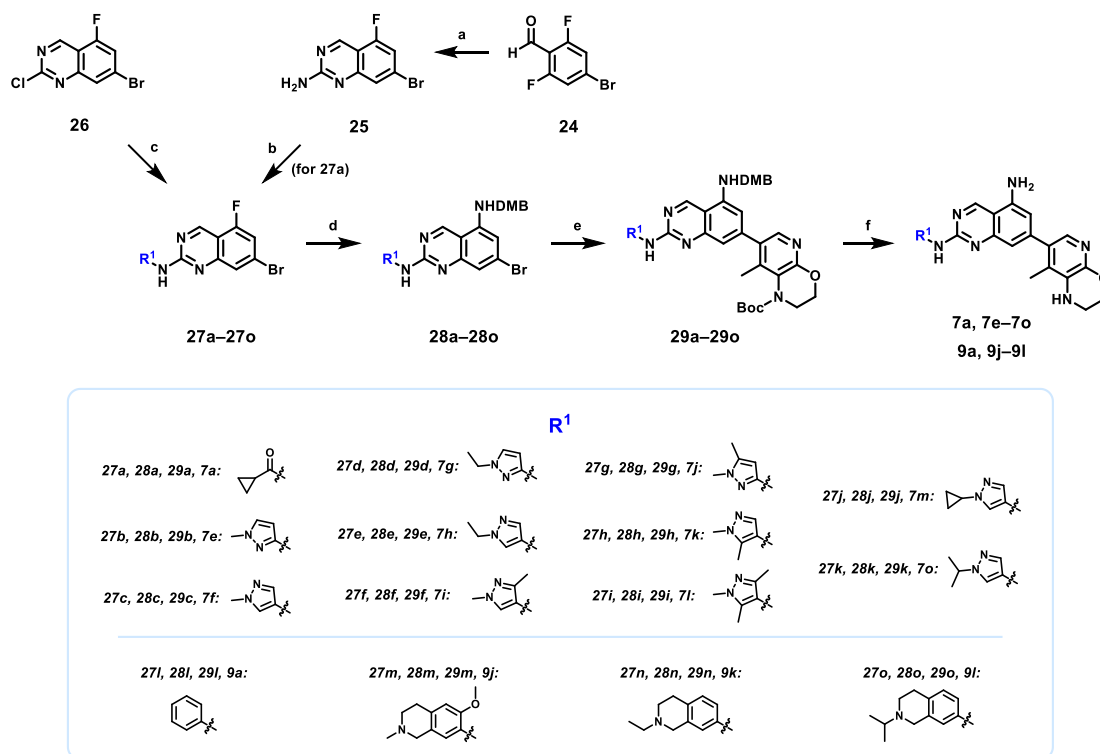
3. Chemistry

The syntheses of several key intermediates were carried out as outlined in **Scheme 1**. 7-Bromo-2-chloro-5-fluoroquinazoline (**14**) was prepared by five steps. Benzylic bromination of commercially available **10** yielded benzyl bromide derivative **11**, which then underwent an oxidation using N-methylmorpholine N-oxide followed by nitro group reduction to give **13**. The 2-nitrobenzaldehyde moiety of **13** was further cyclized with urea to construct the quinazoline skeleton, and finally, chlorination of the obtained quinazolin-2-ol crude provided the desired Intermediate **14**. 1-Cyclopropyl-1H-pyrazol-4-amine **17** was synthesized *via* Chan-Lam coupling reaction followed by catalytic hydrogenation starting from 4-nitro-1H-pyrazole (**15**). As for the synthesis of bicyclic boronic acid ester **23**, S_NAr substitution of commercially available **18** furnished intermediate **19**, which further went through a spontaneous intramolecular cyclization during the nitro group reduction to afford **20**. Afterwards, the lactam derivative **20** was reduced by borane and introduced with a Boc protecting group to produce **22**. Lastly, Miyaura borylation converted the heteroaryl bromide **22** to boronic acid pinacol ester **23**.



Scheme 1. Synthesis of intermediates **14**, **17** and **23**. Reagents and conditions: (a) Benzoyl peroxide, NBS, CCl₄, 80 °C, 18 h; (b) N-methylmorpholine N-oxide, CH₃CN, rt, 6 h; (c) iron powder, acetic acid, EtOH, 0 °C, 2 h; (d) urea, 140 °C, 2 h; (e) POCl₃, reflux, 6 h; (f) cyclopropylboronic acid, Cu(OAc)₂, 2,2'-bipyridine, Na₂CO₃, 1,2-dichloroethane, 70 °C, 10 h; (g) H₂, Pd/C, MeOH, rt, 6 h; (h) ethyl glycolate, DBU, 60 °C, 8 h; (i) zinc powder, acetic acid, EtOH, 100 °C, 1 h; (j) BH₃·THF, anhydrous THF, 0 °C to rt, overnight; (k) LiHMDS, Boc₂O, anhydrous THF, 0 °C to rt, 2 h; (l) bis(pinacolato)diboron, Pd(dppf)Cl₂·CH₂Cl₂, KOAc, 1,4-dioxane, 90 °C, 2.5 h.

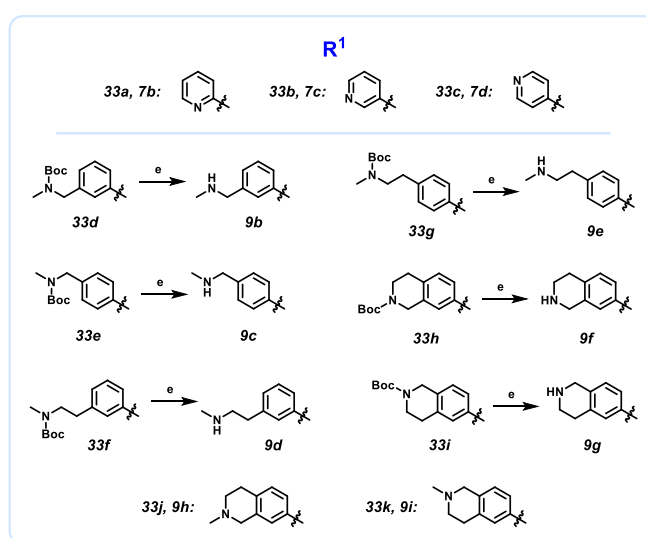
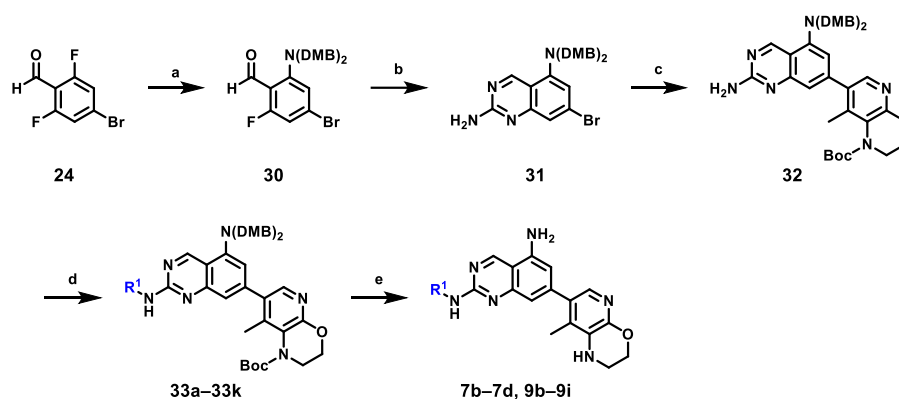
The synthetic route of **7a** are shown in **Scheme 2**, inspired by the method reported by Taylor *et al*, we also constructed the quinazoline skeleton by conducting a ring-closure reaction of 4-bromo-2,6-difluorobenzaldehyde (**24**) with diguanidinium carbonate[36]. The subsequent acylation and nucleophilic attack by 2,4-dimethoxybenzylamine converted quinazolin-2-amine **25** to **28a**. Next, Suzuki coupling reaction enabled the connection between **28a** and boronic acid pinacol ester **23**, and the eventual deprotection using TFA afford compound **7a**. When preparing compounds **7e–7o**, **9a** and **9j–9l**, acid-promoted S_NAr substitutions were utilized for the regioselective installations of these aminopyrazoles and arylamines, and the later steps were same as that of **7a**.



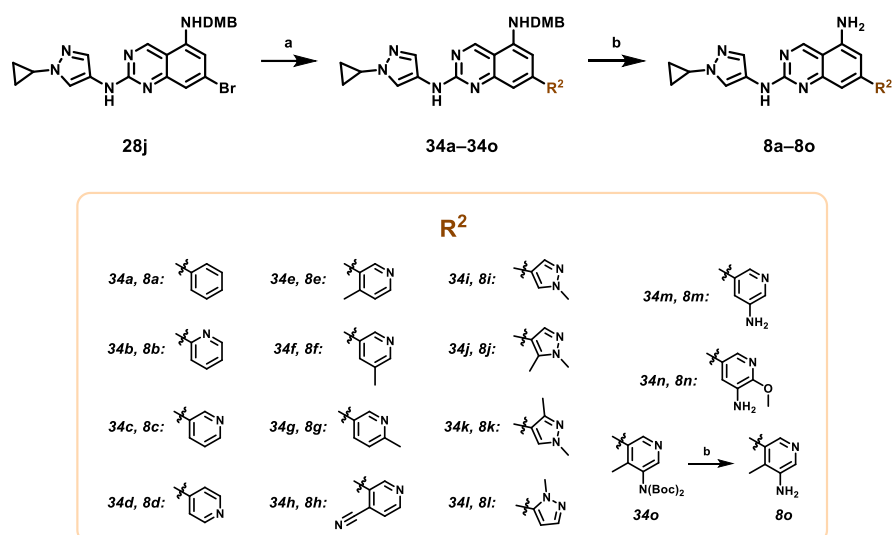
Scheme 2. Synthesis of compounds **7a**, **7e–7o**, **9a** and **9j–9l**. Reagents and conditions: (a) diguanidinium carbonate, DIPEA, NMP, 100 °C, 16 h; (b) cyclopropanecarbonyl chloride, pyridine, 0 °C to rt, 2 h; (c) for **27b–27l** (except **27j**): appropriate aminopyrazole or aniline, HCl, EtOH, 120 °C or 80 °C, 5 h; for **27j** and **27m–27o**: **17** or appropriate arylamine, HCl, i-PrOH, 85 °C, 4 h; (d) 2,4-dimethoxybenzylamine, K₂CO₃, DMF, 100 °C, 16 h; (e) **23**, Pd(dppf)Cl₂·CH₂Cl₂, K₂CO₃, 1,4-dioxane/H₂O, 80 °C, overnight; (f) TFA, rt, 2 h.

When R¹ substituents were pyridyls or the rest of the aryl groups, an alternative route as **Scheme 3** depicts was employed. After mono-substitution of 4-bromo-2,6-difluorobenzaldehyde (**24**) with bis(2,4-dimethoxybenzyl)amine, the quinazoline skeleton was constructed by a similar method to that of **25**. Then, a Suzuki reaction between the obtained **31** and the boronic acid pinacol ester **23** occurred, followed by Buchwald coupling reactions with various aryl or heteroaryl halides to furnish **33a–33k**. Finally, deprotections of multiple protecting groups yielded the target compounds. Starting from intermediate **28j**, compounds **8a–8o** were efficiently synthesized *via* a

two-step reaction process including Suzuki reaction and deprotection (**Scheme 4**).



Scheme 3. Synthesis of compounds **7b – 7d**, **9b–9i**. Reagents and conditions: (a) bis(2,4-dimethoxybenzyl)amine, K_2CO_3 , DMF, 50 °C, 8 h; (b) diguanidinium carbonate, DIPEA, NMP, 140 °C, 16 h; (c) **23**, $Pd(dppf)Cl_2 \cdot CH_2Cl_2$, K_2CO_3 , 1,4-dioxane/ H_2O , 80 °C, overnight; (d) appropriate chloropyridine, bromopyridine or aryl bromide, $Pd_2(dba)_3$, XantPhos, CS_2CO_3 , 1,4-dioxane, 80 °C or 95 °C (for **33j**), overnight; (e) TFA, rt, 2 h.



Scheme 4. Synthesis of compounds **8a–8o**. Reagents and conditions: (a) appropriate boronic acid or boronic acid pinacol ester, Pd(dppf)Cl₂·CH₂Cl₂, K₂CO₃, 1,4-dioxane/H₂O, 80 °C, overnight; (b) TFA, rt, 2 h.

4. Conclusions

In summary, inspired by a set of highly potent isoquinoline-3,8-diamine HPK1 inhibitors, we generated the quinazoline-2,5-diamine skeleton and explored the SARs at 2-amino group and C7 position. While carbonyl substituent on the 2-amino group was not matched with our quinazoline core, replacing it with five- or six- membered heterocycles could bring high inhibitory activities. SAR exploration at C7 position shed light on some of the potency determinants. Introducing aliphatic amines as putative Asp101-interacting groups to the 2-aniline moiety yielded several tetrahydroisoquinoline derivatives with further improved activities, among which the most potent **9h** displayed an IC₅₀ value of 2.7 nM in our internal ADP-Glo kinase assay. In Jurkat cells, **9h** could dose-dependently inhibit the phosphorylation of the downstream SLP76, and the inhibitory effect could still be observed even at 3.3 nM. Results from further evaluations using hPBMCs revealed that **9h** could augment the IL-

2 secretion and reverse the PGE2-induced immune suppression. Taken together, our study on these quinazoline-2,5-diamine derivatives provided not only an *in vitro* tool for the community to better understand the HPK1 pharmacology, but also a reliable reference for the later development of HPK1 inhibitors.

5. Experimental section

5.1 Enzymatic assay

ADP-Glo™ Assay for bioluminescent detection was used to evaluate the HPK1 kinase inhibitory activities of inhibitors. HPK1 Kinase Enzyme System was purchased from Promega (Madison, USA) and assays were performed according to the manufacture's instructions. First, a 5 µL kinase reaction was performed including 1 µL inhibitor or 5% DMSO, 3.5 ng HPK1 Kinase, 10 µM ATP and 0.1 µg/µL MBP substrate in 384-well low volume plate, and was incubated the reaction at room temperature for 60 min. Subsequently, 5 µL ADP-Glo™ Reagent was added for 40 minutes at room temperature. Then 10 µL Kinase Detection Reagent was added. After incubating for 30 minutes, the luminescence values were measured using SpectraMax Paradigm and 50% inhibitive concentration (IC₅₀) values were generated by the four-parameter Logit method.

5.2 Western Blot

Jurkat, Clone E6-1 (Acute T cell leukemia cell line) was acquired from American Type Culture Collection (ATCC, USA). Jurkat cells were cultured at 37 °C in a 5% CO₂-humidified atmosphere, maintaining in RPMI-1640 medium with 10% fetal bovine serum (FBS). Jurkat cells were seeded in 12-well plates and treated with

indicated concentrations of compounds the next day. After 2 hours of drug administration, cells were stimulated with anti-human CD3 (5 µg/mL, Biolegend 317326) and anti-human CD28 (2 µg/mL, Biolegend 302934) for 10 minutes. After stimulation, cells were collected, washed and lysed in lysis buffer contained with 5% SDS. Lysate was boiled and analysed by SDS-PAGE (Bio-Rad) and transfer to nitrocellulose membranes (Cytiva), which were then blocked with 5% skim milk in TBST buffer (150 mM NaCl, 20 mM Tris-HCl pH 7.6, 0.1% Tween-20) for 30 min before incubation with primary antibodies at 4 °C overnight. After washing with TBST, membranes were incubated with secondary antibody for 40 min and then washed three times with TBST before adding the West Pico substrate (ThermoFisher Scientific) for detection. Antibodies were phospho-SLP-76 (Ser376) (Cell Signaling Technology 92711), SLP-76 (Cell Signaling Technology 25361) and alpha-tubulin polyclonal antibody (Proteintech 11224-1-AP). Relative band intensity was analysed by Image Lab (Bio-Rad). One-way ANOVA with Fisher's LSD comparisons were used to determine the difference of drug-treating groups vs anti-CD3/28 only group.

5.3 IL-2 production tests of hPBMCs

Human PBMCs were purchased from Shanghai Hycells Co., Ltd and were cultured at 37 °C in a 5% CO₂-humidified atmosphere, maintaining in RPMI-1640 medium with 10% FBS. hPBMCs were seeded in 96-well plate and were treated with HPK1 inhibitors for 1 hours. Cells were then transferred into a plate pre-coated with anti-human CD3 (0.5 µg/mL), fueling with anti-human CD28 (0.5 µg/mL), and further cultured for 48 hours. PGE₂ (5 nM) was added together with anti-human CD28 if

needed. Culture supernatant was collected after 48 hours and IL-2 was tested by ELISA (Biolegend 431804) following the manufacture's instruction. Two-way ANOVA were used to compare effects among several doses of 3 compounds. A mixed-effect analysis were used to compare effectes with or without PGE2. Multipule comparisons were performed by Fisher's LSD multipule comparison. Paried t-test were used to analysis drug effect of individual hPBMC donor.

References

- [1] J. Tang, A. Shalabi, V.M. Hubbard-Lucey, Comprehensive analysis of the clinical immunology landscape, *Ann. Oncol.*, 29 (2018) 84-91. <https://doi.org/10.1093/annonc/mdx755>.
- [2] A.J. Korman, S.C. Garrett-Thomson, N. Lonberg, The foundations of immune checkpoint blockade and the ipilimumab approval decennial, *Nat. Rev. Drug. Discov.*, 21 (2022) 509-528. <https://doi.org/10.1038/s41573-021-00345-8>.
- [3] J.S. Weber, S.P. D'Angelo, D. Minor, F.S. Hodi, R. Gutzmer, B. Neyns, C. Hoeller, N.I. Khushalani, W.H. Miller, C.D. Lao, G.P. Linette, L. Thomas, P. Lorigan, K.F. Grossmann, J.C. Hassel, M. Maio, M. Sznol, P.A. Ascierto, P. Mohr, B. Chmielowski, A. Bryce, I.M. Svane, J.-J. Grob, A.M. Krackhardt, C. Horak, A. Lambert, A.S. Yang, J. Larkin, Nivolumab versus chemotherapy in patients with advanced melanoma who progressed after anti-CTLA-4 treatment (CheckMate 037): a randomised, controlled, open-label, phase 3 trial, *The Lancet Oncology*, 16 (2015) 375-384. [https://doi.org/10.1016/S1470-2045\(15\)70076-8](https://doi.org/10.1016/S1470-2045(15)70076-8).
- [4] R.J. Motzer, B. Escudier, D.F. McDermott, S. George, H.J. Hammers, S. Srinivas, S.S. Tykodi, J.A. Sosman, G. Procopio, E.R. Plimack, D. Castellano, T.K. Choueiri, H. Gurney, F. Donskov, P. Bono, J. Wagstaff, T.C. Gaurer, T. Ueda, Y. Tomita, F.A. Schutz, C. Kollmannsberger, J. Larkin, A. Ravaud, J.S. Simon, L.-A. Xu, I.M. Waxman, P. Sharma, Nivolumab versus Everolimus in Advanced Renal-Cell Carcinoma, *N. Engl. J. Med.*, 373 (2015) 1803-1813. <https://doi.org/10.1056/NEJMoa1510665>.
- [5] H. Borghaei, L. Paz-Ares, L. Horn, D.R. Spigel, M. Steins, N.E. Ready, L.Q. Chow, E.E. Vokes, E. Felip, E. Holgado, F. Barlesi, M. Kohlhäufel, O. Arrieta, M.A. Burgio, J. Fayette, H. Lena, E. Poddubskaya, D.E. Gerber, S.N. Gettinger, C.M. Rudin, N. Rizvi, L. Crinò, G.R. Blumenschein, S.J. Antonia, C. Dorange, C.T. Harbison, F. Graf Finckenstein, J.R. Brahmer, Nivolumab versus Docetaxel in Advanced Nonsquamous Non-Small-Cell Lung Cancer, *N. Engl. J. Med.*, 373 (2015) 1627-1639. <https://doi.org/10.1056/NEJMoa1507643>.
- [6] J.E. Rosenberg, J. Hoffman-Censits, T. Powles, M.S. van der Heijden, A.V. Balar, A. Necchi, N. Dawson, P.H. O'Donnell, A. Balmanoukian, Y. Loriot, S. Srinivas, M.M. Retz, P. Grivas, R.W. Joseph, M.D. Galsky, M.T. Fleming, D.P. Petrylak, J.L. Perez-Gracia, H.A. Burris, D. Castellano, C. Canil, J. Bellmunt, D. Bajorin, D. Nickles, R. Bourgon, G.M. Frampton, N. Cui, S. Mariathasan, O. Abidoye, G.D. Fine, R. Dreicer, Atezolizumab in patients with locally advanced and metastatic urothelial carcinoma who have progressed following treatment with platinum-based chemotherapy: a single-arm, multicentre, phase 2 trial, *The Lancet*, 387 (2016) 1909-1920. [https://doi.org/10.1016/S0140-6736\(16\)00561-4](https://doi.org/10.1016/S0140-6736(16)00561-4).
- [7] H.L. Kaufman, J. Russell, O. Hamid, S. Bhatia, P. Terheyden, S.P. D'Angelo, K.C. Shih, C. Lebbé, G.P. Linette, M. Milella, I. Brownell, K.D. Lewis, J.H. Lorch, K. Chin, L. Mahnke, A. von Heydebreck, J.-M. Cuillerot, P. Nghiem, Avelumab in patients with chemotherapy-refractory metastatic Merkel cell carcinoma: a multicentre, single-group, open-label, phase 2 trial, *The Lancet Oncology*, 17 (2016) 1374-1385. [https://doi.org/10.1016/S1470-2045\(16\)30364-3](https://doi.org/10.1016/S1470-2045(16)30364-3).
- [8] P. Sharma, S. Hu-Lieskovan, J.A. Wargo, A. Ribas, Primary, Adaptive, and Acquired Resistance to Cancer Immunotherapy, *Cell*, 168 (2017) 707-723. <https://doi.org/10.1016/j.cell.2017.01.017>.
- [9] P.S. Hegde, D.S. Chen, Top 10 Challenges in Cancer Immunotherapy, *Immunity*, 52 (2020) 17-35. <https://doi.org/10.1016/j.immuni.2019.12.011>.

- [10] T.K. Kim, E.N. Vandsemb, R.S. Herbst, L. Chen, Adaptive immune resistance at the tumour site: mechanisms and therapeutic opportunities, *Nat. Rev. Drug. Discov.*, 21 (2022) 529-540. <https://doi.org/10.1038/s41573-022-00493-5>.
- [11] D.S. Chen, I. Mellman, Elements of cancer immunity and the cancer-immune set point, *Nature*, 541 (2017) 321-330. <https://doi.org/10.1038/nature21349>.
- [12] J.L. Adams, J. Smothers, R. Srinivasan, A. Hoos, Big opportunities for small molecules in immuno-oncology, *Nat. Rev. Drug. Discov.*, 14 (2015) 603-622. <https://doi.org/10.1038/nrd4596>.
- [13] S.Y. van der Zanden, J.J. Luimstra, J. Neefjes, J. Borst, H. Ovaa, Opportunities for Small Molecules in Cancer Immunotherapy, *Trends Immunol.*, 41 (2020) 493-511. <https://doi.org/10.1016/j.it.2020.04.004>.
- [14] H.C. Chuang, X. Wang, T.H. Tan, MAP4K Family Kinases in Immunity and Inflammation, *Adv. Immunol.*, 129 (2016) 277-314. <https://doi.org/10.1016/bs.ai.2015.09.006>.
- [15] S. Sawasdikosol, S. Burakoff, A perspective on HPK1 as a novel immuno-oncology drug target, *Elife*, 9 (2020) <https://doi.org/10.7554/eLife.55122>.
- [16] J.W. Shui, J.S. Boomer, J. Han, J. Xu, G.A. Dement, G. Zhou, T.H. Tan, Hematopoietic progenitor kinase 1 negatively regulates T cell receptor signaling and T cell-mediated immune responses, *Nat. Immunol.*, 8 (2007) 84-91. <https://doi.org/10.1038/ni1416>.
- [17] S. Alzabin, S. Pyarajan, H. Yee, F. Kiefer, A. Suzuki, S. Burakoff, S. Sawasdikosol, Hematopoietic progenitor kinase 1 is a critical component of prostaglandin E2-mediated suppression of the anti-tumor immune response, *Cancer Immunol. Immunother.*, 59 (2010) 419-429. <https://doi.org/10.1007/s00262-009-0761-0>.
- [18] S. Hernandez, J. Qing, R.H. Thibodeau, X. Du, S. Park, H.M. Lee, M. Xu, S. Oh, A. Navarro, M. Roose-Girma, R.J. Newman, S. Warming, M. Nannini, D. Sampath, J.M. Kim, J.L. Grogan, I. Mellman, The Kinase Activity of Hematopoietic Progenitor Kinase 1 Is Essential for the Regulation of T Cell Function, *Cell Rep.*, 25 (2018) 80-94. <https://doi.org/10.1016/j.celrep.2018.09.012>.
- [19] J. Liu, J. Curtin, D. You, S. Hillerman, B. Li-Wang, R. Eraslan, J. Xie, J. Swanson, C.P. Ho, S. Oppenheimer, B.M. Warrack, C.A. McNaney, D.M. Nelson, J. Blum, T. Kim, M. Fereshteh, M. Reily, P. Shipkova, A. Murtaza, M. Sanjuan, J.T. Hunt, L. Salter-Cid, Critical role of kinase activity of hematopoietic progenitor kinase 1 in anti-tumor immune surveillance, *PLoS One*, 14 (2019) e0212670. <https://doi.org/10.1371/journal.pone.0212670>.
- [20] X. Wang, J.P. Li, H.K. Kuo, L.L. Chiu, G.A. Dement, J.L. Lan, D.Y. Chen, C.Y. Yang, H. Hu, T.H. Tan, Down-regulation of B cell receptor signaling by hematopoietic progenitor kinase 1 (HPK1)-mediated phosphorylation and ubiquitination of activated B cell linker protein (BLNK), *J. Biol. Chem.*, 287 (2012) 11037-11048. <https://doi.org/10.1074/jbc.M111.310946>.
- [21] S. Alzabin, N. Bhardwaj, F. Kiefer, S. Sawasdikosol, S. Burakoff, Hematopoietic progenitor kinase 1 is a negative regulator of dendritic cell activation, *J. Immunol.*, 182 (2009) 6187-6194. <https://doi.org/10.4049/jimmunol.0802631>.
- [22] ClinicalTrials.gov, Safety and Efficacy Study Of CFI-402411 in Subjects With Advanced Solid Malignancies. <https://clinicaltrials.gov/ct2/show/NCT04521413?term=NCT04521413&draw=2&rank=1>, 2022 (accessed 26 Jul 2022).
- [23] ClinicalTrials.gov, BGB-15025 Alone and in Combination With Anti-PD-1 Monoclonal Antibody Tislelizumab in Participants With Advanced Solid Tumors. <https://clinicaltrials.gov/ct2/show/NCT04649385?term=NCT04649385&draw=2&rank=1>, 2022

(accessed 26 Jul 2022).

[24] ClinicalTrials.gov, A Study of NDI 1150-101 in Patients With Solid Tumors. <https://clinicaltrials.gov/ct2/show/NCT05128487?term=NCT05128487&draw=2&rank=1>, 2022 (accessed 26 Jul 2022).

[25] ClinicalTrials.gov, Phase I Study, Evaluating the Safety, Pharmacokinetics and Efficacy of PRJ1-3024 in Subjects With Advanced Solid Tumors. <https://clinicaltrials.gov/ct2/show/NCT05159700?term=NCT05159700&draw=2&rank=1>, 2022 (accessed 26 Jul 2022).

[26] ClinicalTrials.gov, PF-07265028 As Single Agent And In Combination With Sasanlimab in Advanced or Metastatic Solid Tumors. <https://clinicaltrials.gov/ct2/show/NCT05233436?term=NCT05233436&draw=2&rank=1>, 2022 (accessed 26 Jul 2022).

[27] ClinicalTrials.gov, A Phase I/II Study to Evaluate the Safety, Pharmacokinetics and Efficacy of PRJ1-3024 in Subjects With Advanced Solid Tumors. <https://clinicaltrials.gov/ct2/show/NCT05315167?term=NCT05315167&draw=2&rank=1>, 2022 (accessed 26 Jul 2022).

[28] E.C. Yu, J.L. Methot, X. Fradera, C.A. Lesburg, B.M. Lacey, P. Siliphaivanh, P. Liu, D.M. Smith, Z. Xu, J.A. Piesvaux, S. Kawamura, H. Xu, J.R. Miller, M. Bittinger, A. Pasternak, Identification of Potent Reverse Indazole Inhibitors for HPK1, ACS Med. Chem. Lett., 12 (2021) 459-466. <https://doi.org/10.1021/acsmchemlett.0c00672>.

[29] B.K. Chan, E. Seward, M. Lainchbury, T.F. Brewer, L. An, T. Blench, M.W. Cartwright, G.K.Y. Chan, E.F. Choo, J. Drummond, R.L. Elliott, E. Gancia, L. Gazzard, B. Hu, G.E. Jones, X. Luo, A. Madin, S. Malhotra, J.G. Moffat, J. Pang, L. Salphati, C.J. Sneeringer, C.E. Stivala, B. Wei, W. Wang, P. Wu, T.P. Heffron, Discovery of Spiro-azaindoline Inhibitors of Hematopoietic Progenitor Kinase 1 (HPK1), ACS Med. Chem. Lett., 13 (2022) 84-91. <https://doi.org/10.1021/acsmchemlett.1c00473>.

[30] B.A. Vara, S.M. Levi, A. Achab, D.A. Candito, X. Fradera, C.A. Lesburg, S. Kawamura, B.M. Lacey, J. Lim, J.L. Methot, Z. Xu, H. Xu, D.M. Smith, J.A. Piesvaux, J.R. Miller, M. Bittinger, S.H. Ranganath, D.J. Bennett, E.F. DiMauro, A. Pasternak, Discovery of Diaminopyrimidine Carboxamide HPK1 Inhibitors as Preclinical Immunotherapy Tool Compounds, ACS Med. Chem. Lett., 12 (2021) 653-661. <https://doi.org/10.1021/acsmchemlett.1c00096>.

[31] J. Si, X. Shi, S. Sun, B. Zou, Y. Li, D. An, X. Lin, Y. Gao, F. Long, B. Pang, X. Liu, T. Liu, W. Chi, L. Chen, D.S. Dimitrov, Y. Sun, X. Du, W. Yin, G. Gao, J. Min, L. Wei, X. Liao, Hematopoietic Progenitor Kinase1 (HPK1) Mediates T Cell Dysfunction and Is a Druggable Target for T Cell-Based Immunotherapies, Cancer Cell, 38 (2020) 551-566 e511. <https://doi.org/10.1016/j.ccell.2020.08.001>.

[32] A.P. Degnan, G.K. Kumi, C.W. Allard, E.V. Araujo, W.L. Johnson, K. Zimmermann, B.C. Pearce, S. Sheriff, A. Futran, X. Li, G.A. Locke, D. You, J. Morrison, K.E. Parrish, C. Stromko, A. Murtaza, J. Liu, B.M. Johnson, G.D. Vite, M.D. Wittman, Discovery of Orally Active Isofuranones as Potent, Selective Inhibitors of Hematopoietic Progenitor Kinase 1, ACS Med. Chem. Lett., 12 (2021) 443-450. <https://doi.org/10.1021/acsmchemlett.0c00660>.

[33] B.M. Lacey, Z. Xu, X. Chai, J. Laskey, X. Fradera, P. Mittal, S. Mishra, J. Piesvaux, P. Saradjian, L. Shaffer, G. Vassileva, C. Gerdt, Y. Wang, H. Ferguson, D.M. Smith, J. Ballard, S. Wells, R. Jain, U. Mueller, G. Addona, I. Kariv, J.L. Methot, M. Bittinger, S. Ranganath, R. McLeod, A. Pasternak, J.R. Miller, H. Xu, Development of High-Throughput Assays for Evaluation of

Hematopoietic Progenitor Kinase 1 Inhibitors, *SLAS Discov*, 26 (2021) 88-99.

<https://doi.org/10.1177/2472555220952071>.

[34] B. Chan, J. Drobnick, L. Gazzard, T. Heffron, J. Liang, S. Malhotra, R. Mendonca, N. Rajapaksa, C. Stivala, J. Tellis, W. Wang, B. Wei, A. Zhou, M.W. Cartwright, M. Lainchbury, E. Gancia, E. Seward, A. Madin, D. Favor, K.C. Fong, Y. Hu, A. Good, Preparation of isoquinolines as inhibitors of HPK1 useful for treatment of cancer, WO2018183964A1, 4 Oct 2018.

[35] R. Kurczab, P. Sliwa, K. Rataj, R. Kafel, A.J. Bojarski, Salt Bridge in Ligand-Protein Complexes-Systematic Theoretical and Statistical Investigations, *J. Chem. Inf. Model.*, 58 (2018) 2224-2238. <https://doi.org/10.1021/acs.jcim.8b00266>.

[36] N.J. Taylor, E. Emer, S. Preshlock, M. Schedler, M. Tredwell, S. Verhoog, J. Mercier, C. Genicot, V. Gouverneur, Derisking the Cu-Mediated (18)F-Fluorination of Heterocyclic Positron Emission Tomography Radioligands, *J. Am. Chem. Soc.*, 139 (2017) 8267-8276. <https://doi.org/10.1021/jacs.7b03131>.